Lasers in Manufacturing Conference 2021

3D printing of high-density copper parts using common NIR CW laser systems at moderate powers

Hagen Kohl[a,*], Lisa Schade[a], Gabor Matthäus[a], Tobias Ullsperger[a], Burak Yürekli[a], Brian Seyfarth[a,b], Bernd Braun[c], Stefan Nolte[a,b]

[a]*Institute of Applied Physics, Abbe Center of Photonics, Friedrich Schiller University Jena, Albert-Einstein-Straße 15, 07745 Jena, Germany*
[b]*Fraunhofer Institute for Applied Optics and Precision Engineering IOF, Center of Excellence in Photonics, Albert-Einstein-Straße 7, 07745 Jena, Germany*
[c]*Nuremberg Institute of Technology Georg Simon Ohm, Kesslerplatz 12, 90489 Nuremberg, Germany*

Abstract

Additive manufacturing (AM) of pure copper using laser assisted powder bed fusion (LPBF) at a wavelength of 1070 nm is demonstrated. In comparison to established LPBF materials, pure copper exhibits an extremely high reflectivity for wavelengths around 1 µm and the highest thermal conductivity among other AM materials. Although, pure copper is one of the most interesting materials for AM, the interplay of these characteristics still prevents copper to be applied using common laser-based AM machines. In this work, we demonstrate a processing window for 3D-printing of high-density copper parts based on a fiber laser as widely used in common AM machines. These achievements were obtained with the help of a self-developed numerical model that guided our experimental studies during the LPBF process. After process optimization, relative densities over 99 % could be demonstrated without the help of intense preheating or post processing like hot isostatic pressing.

Keywords: Additive manufacturing; Powder bed fusion; 3D printing; Pure copper; Numerical simulation;

1. Intoduction

Additive manufacturing (AM) based on the laser assisted powder bed fusion (LPBF) has become an established process in the industrial environment over the last decade. The layer-by-layer process allows the production of highly complex components which cannot be produced by conventional manufacturing

* Corresponding author. Tel.: +49 3641 947825; fax: +49 3641 947802 .
E-mail address: hagen.kohl@uni-jena.de.

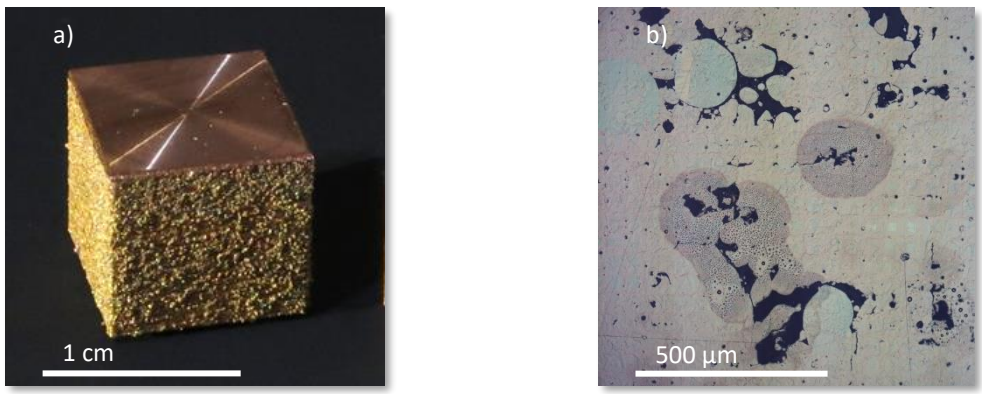

Fig. 1. a) First fabricated cubic copper specimen using LPBF and b) excerpt of its cross section using a light microscope.

methods such as machining or metal casting. These complex structures together with a high thermal conductivity would give the opportunity to fabricate, e.g., highly efficient cooling structures as presented by Sinico et al., 2019. For that reason, attempts are being made to establish pure copper as a material for additive manufacturing [Sinico et al., 2019, Kaden et al., 2017, Tran et.al., 2019, Stoll et al., 2020] recently. However, the AM process of pure copper is rather difficult for various reasons. For example, there is the high reflectivity (bulk 90 % to 99 %) in the infrared spectral range around 1 µm, which is the commonly used spectral range for LPBF of metals. The high reflectance together with the high thermal conductivity of around 390 W m^{-1} K^{-1} [Hust et al., 1984] significantly hinders the copper melting process. Furthermore, the reflectance and thermal conductivity change drastically at the phase transition from solid to liquid [Blom et al., 2003] which in general leads to an unstable and chaotic melting during processing. This yields a poor surface quality (Fig. 1 a) and a reduced density which refers to unmolten particles and lack of fusion effects (Fig. 1 b). Furthermore, this leads to a weakening in strength, decrease in shape accuracy and a reduction of the thermal and electrical conductance.

In order to optimize the LPBF process of pure copper it is mandatory to obtain a better understanding of the dynamic processes in the melt pool which are hardly accessible on an experimental basis. Therefore, a numerical simulation of the melting process for copper is one approach in order to understand the underlying processes and thereby to significantly improve the melting process.

2. Experimental Setup

Fig. 2 shows the schematic of the setup used in our experiments. It was developed in-house and is highly customizable. As a laser source an SPI redPOWER® 500 W continuous wave fiber laser is utilized which was thankfully provided by the TRUMPF GmbH & Co. KG. The laser delivers up to 500 W of laser output power at a wavelength of 1070 nm. The beam position is controlled by a SCANLAB intelliSCAN 14 galvanometer scanner together with a 160 mm F-theta lens whereby a laser spot diameter of 30 µm is obtained at the powder surface. To prevent oxidation the process chamber can be flooded with different inert gases. The shown specimens were fabricated under a nitrogen atmosphere with a residual oxygen content below 0.5 %.

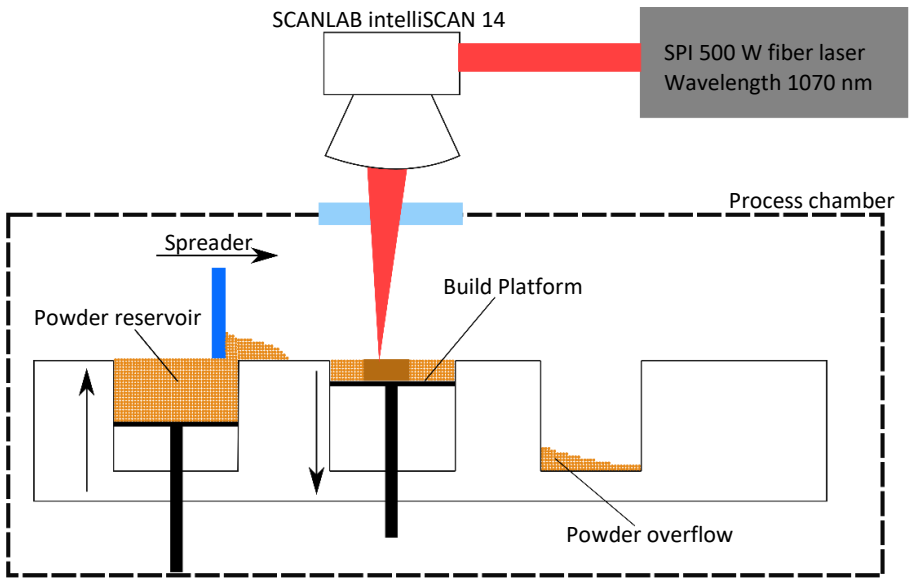

Fig. 2. Schematic of the LPBF-Setup used in the experiments.

3. Powder characteristics

Process parameters and the quality of the fabrication results are highly dependent on the powder characteristics i.e., the powder reflectance, thermal conductivity, and the achieved bulk density. To measure the reflectivity and thermal conductivity of our powders a setup as illustrated in Fig. 3 was realized.

A powder specimen is attached to the sample port of the integrating sphere using a polytetrafluoroethylene (PTFE) holder. To avoid any oxidation effects the whole integrating sphere is filled with nitrogen gas. To avoid any modifications of the powder during the measurement the beam diameter at the powder surface was chosen to be 3 mm and the laser power was limited to a maximum of around 2 W. Photodiode 1 in the setup is used to trigger the measurement and to monitor the power during the exposure time of 0.5 s to account for any power fluctuations of the laser. Photodiode 2 at the detector port of the integrating sphere captures the reflected and scattered light. By comparing the signal of the Photodiode 2 to the signal of a reference with a known reflectivity the average reflectance over many powder particles can be determined.

Using a thermocouple type K within the powder and an oscilloscope the temporal temperature response in the powder is measured around 2.5 mm below the surface. A corresponding temporal temperature profile is also illustrated in Fig. 3. To determine the thermal conductivity of the powder using the temporal temperature response a transient finite element (FE) model of the experiment was implemented which only accounts for the heat conduction in the powder and the PTFE holder. By searching the best fit of the temporal temperature response of the simulation and the experimental data the thermal conductivity of the powder is determined.

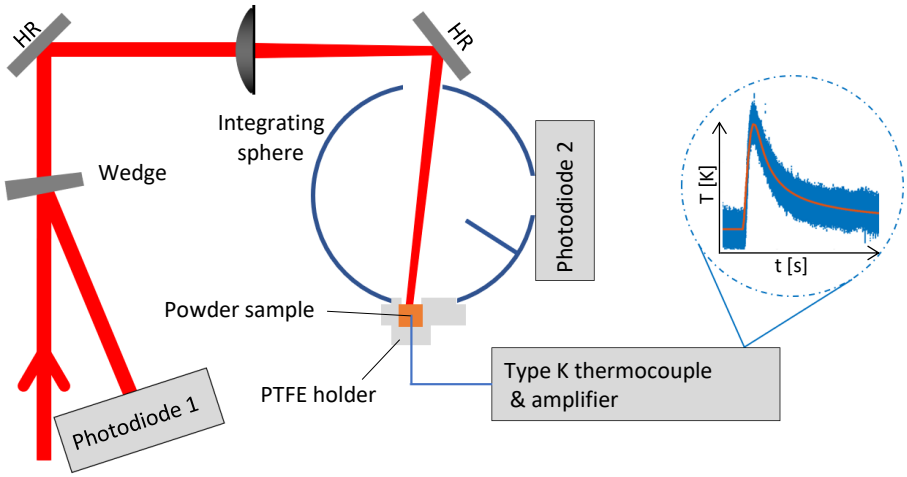

Fig. 3. Schematic of the powder characterization setup.

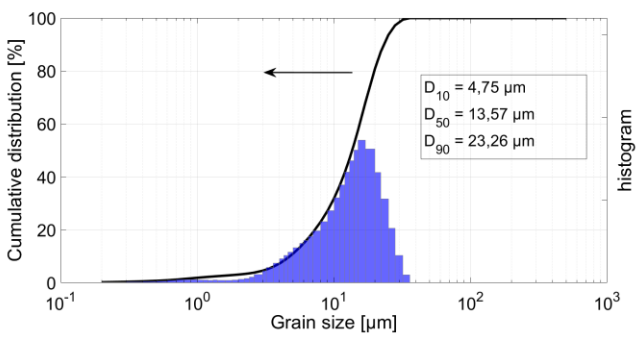

Fig. 4. Particle size distribution of the pure copper powder manufactured by TLS-Technik GmbH.

For all experiments a pure copper powder manufactured by TLS Technik GmbH was used. The spherical powder possesses a purity of 99.7 % and a mean diameter of around 14 µm, a detailed particle size distribution is given in Fig. 4. For this powder a reflectivity of 56 % and a thermal conductivity of 0.19 W m^{-1} K^{-1} was measured at relative bulk density of 56 %. In the literature reflectivity values for copper powders are reported to 59 % and 70 % [Tolochko et al., 2000, Sinico et al., 2019]. Nevertheless, these values are hardly comparable since reference [Tolochko et al., 2000] does not contain any information on the particle size and in reference [Sinico et al., 2019] no bulk density values are given.

It is worth to highlight the difference in the thermal conductivity of the copper powder and copper bulk material with around 390 W m^{-1} K^{-1} [Hust et al., 1984]. The difference of around three orders of magnitude makes a homogeneous melting of already manufactured areas and new powder very difficult and thus lack of fusion effects are more likely to occur.

4. Numerical model

In order to gain sufficient understanding of the mechanisms involved during laser fusion a numerical model of the LPBF process was implemented which allows to investigate the influence of individual parameters. The

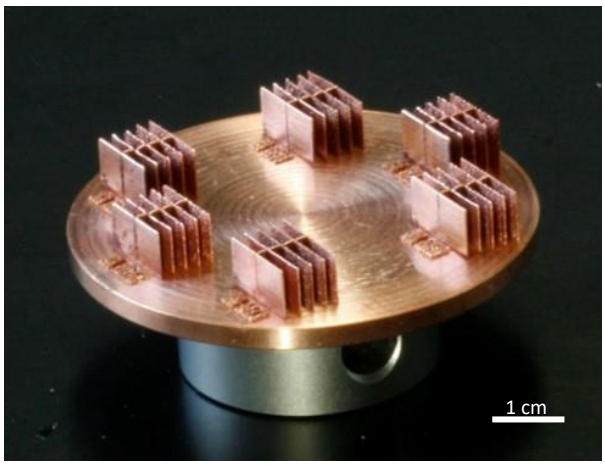

Fig. 5. Thin-wall structures fabricated by LPBF to evaluate the process.

simulation represents the whole process in two stages. In the first stage, a discrete element method (DEM) model accounts for the powder spreading process by calculating the particle-particle interactions based on a Hertzian contact mechanics model, as it is commonly used to model flows of granular materials [Brilliantov et al., 1996, Silbert et al., 2001]. This simulation gives a close to realistic powder distribution which is then used in the second stage to simulate the hydrodynamic flow of the melt pool. Our model is based on a formulation first introduced by Ki et al., 2002, which describes the melt pool dynamics of laser keyhole welding. We adapted the model to match the LPBF process with pure copper. Therefore, the process is represented by combining the incompressible Navier-Stokes equations, the heat transfer equation for fluids and the level-set method to distinguish between air and copper. Between solid and liquid phase, it is distinguished using temperature dependent material parameters. To account for the latent heat during the phase change from solid to liquid the apparent heat capacity method [Comini et al., 1974] is used. The laser heat source is approximated by a Gaussian distributed heat source on the material interface represented by a smoothed delta function.

5. Results and discussion

Evaluating our simulation results we found that the flow velocity of the liquid copper is reduced if the layer height is decreased, whereby a more homogenous melting is achieved, and the amount of spatters is reduced.

It was also found that a stable process is achieved when the laser parameters are chosen to slightly exceed the vaporization temperature of copper, so that a small but stable vapor capillary is formed. Thereby the keyhole is always preceded by a front of molten material, such that the laser only interacts with already molten material. This indicates that the rapid change in reflectivity, described earlier, does not interfere with the stability of the process. In other words, the LPBF using pure copper is stable close to the lower limit of the keyhole regime. Applying the findings to our experimental studies the fabrication results were significantly improved.

Fig. 5 exemplarily shows first successfully fabricated thin-walled structures consisting out of single melting traces produced at laser output powers of 120 W, 140 W, 160 W, 180 W, 200 W, 220 W, laser scanning speeds of 100 mm s^{-1}, 250 mm s^{-1}, 500 mm s^{-1}, 750 mm s^{-1}, and 1000 mm s^{-1} and a layer height 50 µm. For further investigations, these samples were embedded in epoxy resin, wet sanded and mechanically and chemically polished. As shown in Fig. 6 this treatment makes the melt pool visible and also shows defects within the

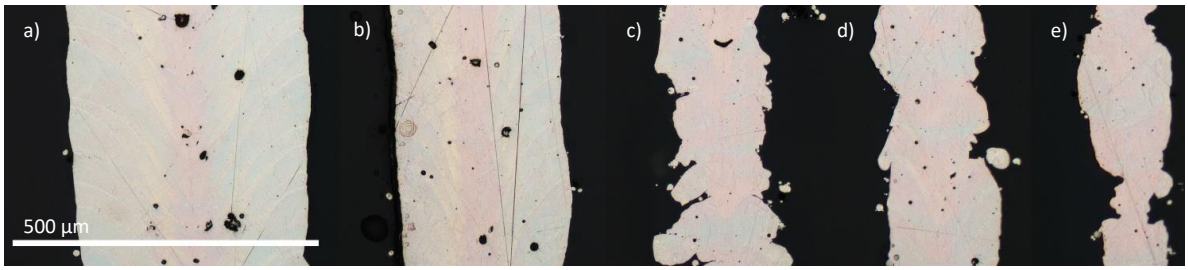

Fig. 6. Cross sections of single lines made by the LPBF process with pure copper at a laser power of 220 W and a layer height of 50 µm for the laser scanning speeds a) 100 mm s^{-1}, b) 250 mm s^{-1}, c) 500 mm s^{-1}, d) 750 mm s^{-1}, and d) 1000 mm s^{-1}.

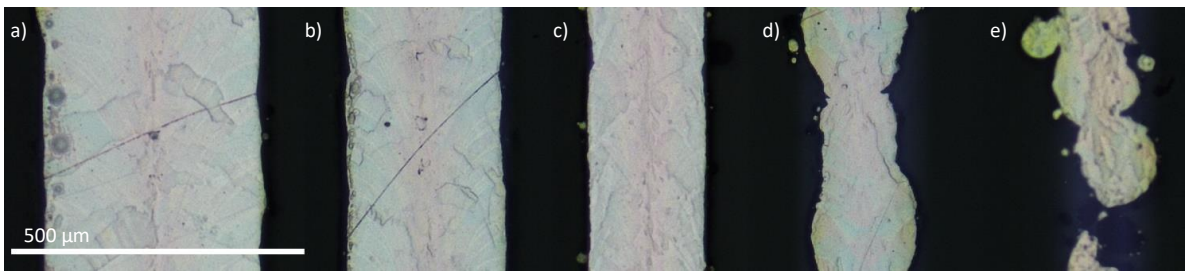

Fig. 7. Cross sections of single lines made by the LPBF process with pure copper at a laser power of 220 W and a layer height of 25 µm for the laser scanning speeds a) 100 mm s^{-1}, b) 250 mm s^{-1}, c) 500 mm s^{-1}, d) 750 mm s^{-1}, and d) 1000 mm s^{-1}.

structures. Here, a laser power of 220 W and scanning speeds between 100 mm s^{-1} and 1000 mm s^{-1} were chosen. In the next step, according to our simulations, the layer height was reduced to stabilize the melt pool. Thereby the cavities within a single melt line could be minimized as shown by Fig. 7. An overview of the line width as a function of the laser power for different laser scanning speeds is given in Fig. 8. The error bars show the standard deviation of the line width for 24 layers using more than 1000 measurements per line. Thus, a homogeneous melting trace is achieved if the error bar is narrow.

The threshold for homogeneous melting is achieved around 100 W of laser power for the scanning speeds of 100 mm s^{-1}, 250 mm s^{-1}, and 500 mm s^{-1}. For higher scanning speeds a constant line width over multiple layers could not be achieved. It is also worth to mention that after achieving homogeneous melting an increase of laser power does not destabilize the melt track in the tested parameter range.

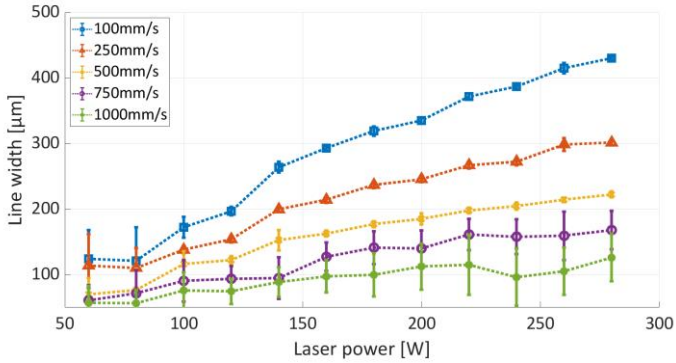

Fig. 8. Line width as a function of the laser power for different laser scanning velocities.

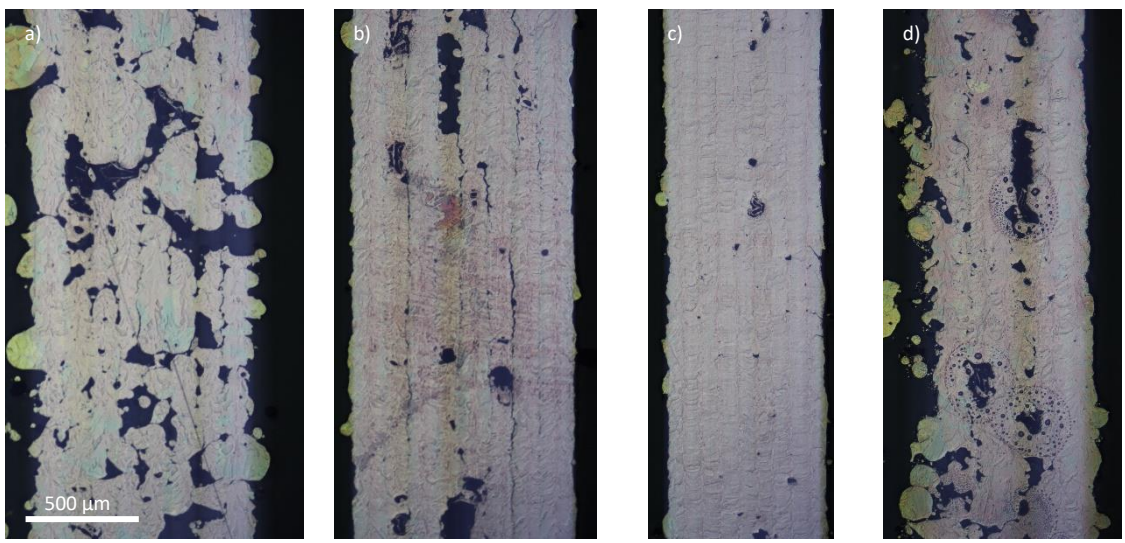

Fig. 9. Volumetric specimen to investigate the influence of the manufacturing parameters on density and the occurrence of lack of fusion effects. For the set of parameters a) laser power 200 W, hatch distance 120 µm, layer height 50 µm; b) laser power 200 W, hatch distance 120 µm, layer height 25 µm; c) laser power 200 W, hatch distance 80 µm, layer height 25 µm; d) laser power 220 W, hatch distance 80 µm, layer height 25 µm. The scanning speed was 500 mm s^{-1} for all specimens.

By applying the same strategy to the fabrication of multiple lines side by side to form a solid, the effect of reducing the layer height to stabilize the melt pool is even more significant compared to the single-walled test specimens. This behavior is well illustrated by the cross sections given in Fig. 9 a) for a layer height of 50 µm and Fig. 9 b) for 25 µm were the number of cavities is reduced. To avoid the lack of fusion effects between the individual lines, mainly caused by the huge difference in the thermal conductivity of the copper powder and copper bulk material, an optimization regarding laser power and hatch distance was performed.

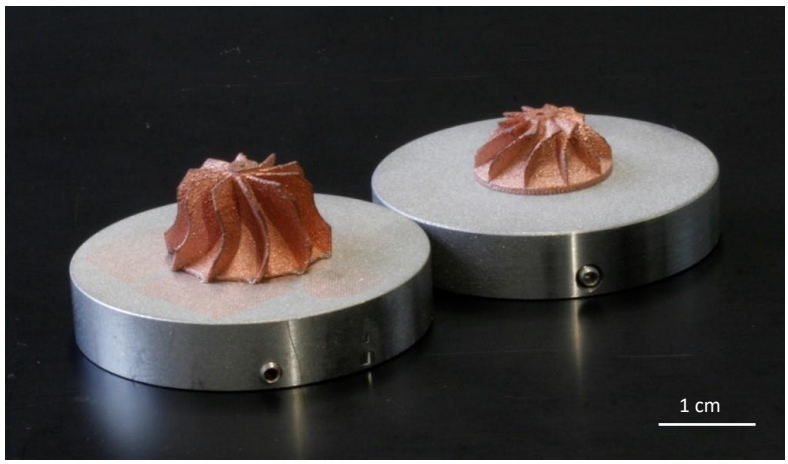

Fig. 10. Additively manufactured demonstrator structures using LPBF at a laser wavelength in the NIR range (1070 nm).

The best result with a relative density of 99 % was achieved for a scanning speed of 500 mm s^{-1}, a hatch spacing of 80 µm, and a laser power of 200 W shown in Fig. 9 c). At this set of parameters, the track overlap corresponds to 60 %. Therefore, the laser interacts primarily with the already processed areas. As shown by Fig. 9 d) the optimal processing window is narrow, since a small increase in laser power already leads to a destabilization of the process, leading to a decrease in density, surface quality, and geometric accuracy. These results demonstrate that it is quite challenging to fabricate parts combining a high homogeneous density with complex geometries i.e., where areas with a very fine structure are surrounded by regions with a high thermal mass. The high thermal conductivity of copper leads to the fact that the heat accumulation during the process depends significantly on the geometry and requires the adjustment of the laser power.

Nevertheless, a good fabrication result could be achieved as shown by the demonstrators in Fig. 10. These structures show, that the fabrication of high aspect ratio parts combining a high level of density together with a high shape accuracy and surface quality is possible.

6. Conclusion

The additive manufacturing of pure copper poses challenges due to the chaotic absorptivity during fusion and the increased thermal conductivity. However, as has been shown, the production of pure copper parts is successful at a wavelength in the near infrared range around 1 µm if the fabrication parameters are chosen correctly. In this work, a wide field of parameters was identified based on single walled test specimens, which makes it possible to manufacture continuous melt tracks of homogeneous width. Furthermore, parameters for thin-walled structures consisting of multiple lines were presented, for which a relative density of 99 % was achieved. Those densities together with a high shape accuracy and surface quality were achieved with the help of a validated multiscale numerical model of the LPBF process. These results demonstrate that the fabrication of high-density copper parts using a fiber laser system as widely used in common AM machines is possible.

Acknowledgements

We gratefully acknowledge support by the German Research Foundation (DFG) within the Priority Program (SPP) 2122 “Materials for Additive Manufacturing (MATframe)” (NO462/13-1) and the German Federal Ministry of Education and Research (BMBF) within the project AM-OPTICS (02P15B203). Lisa Schade acknowledges support by TRUMPF Laser GmbH. Brian Seyfarth likes to acknowledge the Center of Excellence in Photonics of the Fraunhofer Institute for Applied Optics and Precision Engineering (IOF).

References

A. Blom, P. Dunias, P. van Engen, W. Hoving and J. de Kramer, "Process spread reduction of laser microspot welding of thin copper parts using real-time control," in Photon Processing in Microelectronics and Photonics II, 2003.

G. Comini, S. D. Guidice, R. W. Lewis and O. C. Zienkiewicz, "Finite element solution of non-linear heat conduction problems with special reference to phase change," International Journal for Numerical Methods in Engineering, vol. 8, p. 613–624, 1974.

H. Ki, J. Mazumder and P. S. Mohanty, "Modeling of laser keyhole welding: Part I. mathematical modeling, numerical methodology, role of recoil pressure, multiple reflections, and free surface evolution," Metallurgical and Materials Transactions A, vol. 33, p. 1817–1830, 6 2002.

J. G. Hust and A. B. Lankford, "Thermal conductivity of aluminum, copper, iron, and tungsten for temperatures from 1 K to the melting point," 1984.

L. E. Silbert, D. Ertaş, G. S. Grest, T. C. Halsey, D. Levine and S. J. Plimpton, "Granular flow down an inclined plane: Bagnold scaling and rheology," Physical Review E, vol. 64, 10 2001.

L. Kaden, G. Matthäus, T. Ullsperger, H. Engelhardt, M. Rettenmayr, A. Tünnermann and S. Nolte, "Selective laser melting of copper using ultrashort laser pulses," Applied Physics A, vol. 123, 8 2017.

M. Sinico, G. Cogo, M. Benettoni, I. Calliari and A. Pepato, "Influence of Powder Particle Size Distribution on the printability of Pure Copper for Selective Laser Melting," in Proceedings of the 30th Annual InternationalSolid Freeform Fabrication Symposium, 2019.

N. K. Tolochko, Y. V. Khlopkov, S. E. Mozzharov, M. B. Ignatiev, T. Laoui and V. I. Titov, "Absorptance of powder materials suitable for laser sintering," Rapid Prototyping Journal, vol. 6, p. 155–161, 9 2000.

N. V. Brilliantov, F. Spahn, J.-M. Hertzsch and T. Pöschel, "Model for collisions in granular gases," Physical Review E, vol. 53, p. 5382–5392, 5 1996.

T. Q. Tran, A. Chinnappan, J. K. Y. Lee, N. H. Loc, L. T. Tran, G. Wang, V. V. Kumar, W. A. D. M. Jayathilaka, D. Ji, M. Doddamani and S. Ramakrishna, "3D Printing of Highly Pure Copper," Metals, vol. 9, p. 756, 7 2019.

T. Stoll, P. Trautnitz, S. Schmiedeke, J. E. Franke and N. Travitzky, "Process development for laser powder bed fusion of pure copper," in Laser 3D Manufacturing VII, 2020.